Published in final edited form as:
Mol Pharm. 2012 December 3; 9(12): 3586–3594. doi:10.1021/mp3005269.

Positron Emission Tomography Imaging of Vascular Endothelial Growth Factor Receptor Expression with ^{61}Cu-Labeled Lysine-Tagged VEGF$_{121}$

Yin Zhang[1,5], **Hao Hong**[2,5], **Gang Niu**[3], **Hector F. Valdovinos**[1], **Hakan Orbay**[2], **Tapas R. Nayak**[2], **Xiaoyuan Chen**[3], **Todd E. Barnhart**[1], and **Weibo Cai**[1,2,4,*]

[1]Department of Medical Physics, University of Wisconsin - Madison, WI, USA

[2]Department of Radiology, University of Wisconsin - Madison, WI, USA

[3]Laboratory of Molecular Imaging and Nanomedicine, National Institute of Biomedical Imaging and Bioengineering, National Institutes of Health, Bethesda, MD, USA

[4]University of Wisconsin Carbone Cancer Center, Madison, WI, USA

Abstract

Overexpression of vascular endothelial growth factor (VEGF) and VEGF receptors (VEGFRs) indicates poor prognosis for cancer patients in a variety of clinical studies. Our goal is to develop a tracer for positron emission tomography (PET) imaging of VEGFR expression using recombinant human VEGF$_{121}$ with three lysine residues fused to the N-terminus (denoted as K$_3$-VEGF$_{121}$), which can facilitate radiolabeling without affecting its VEGFR binding affinity. K$_3$-VEGF$_{121}$ was conjugated with 1,4,7-triazacyclononane-1,4,7-triacetic acid (NOTA) and labeled with ^{61}Cu ($t_{1/2}$: 3.3 h; 62% β^+). The IC$_{50}$ value of NOTA-K$_3$-VEGF$_{121}$ for VEGFR-2 was comparable to K$_3$-VEGF$_{121}$ (1.50 and 0.65 nM, respectively) based on cell binding assay. ^{61}Cu labeling was achieved with good yield (55 ± 10 %) and specific activity (4.2 GBq/mg). Serial PET imaging showed that the 4T1 tumor uptake of ^{61}Cu-NOTA-K$_3$-VEGF$_{121}$ was 3.4 ± 0.5, 4.9 ± 1.0, 5.2 ± 1.0, and 4.8 ± 0.8 %ID/g (n = 4) at 0.5, 2, 4, and 8 h post-injection respectively, which was consistent with biodistribution data measured by gamma counting. Blocking experiments and ex vivo histology confirmed VEGFR specificity of ^{61}Cu-NOTA-K$_3$-VEGF$_{121}$. Extrapolated human dosimetry calculation showed that liver was the organ with the highest radiation dose. The use of ^{61}Cu as the radiolabel is desirable for small proteins like K$_3$-VEGF$_{121}$, which has much higher β^+ branching ratio than the commonly used ^{64}Cu (62% vs. 17%) thereby offering stronger signal intensity and lower tracer dose for PET imaging.

Keywords

Vascular endothelial growth factor (VEGF); VEGF receptor (VEGFR); ^{61}Cu; Positron emission tomography (PET); Tumor angiogenesis; Molecular imaging

Requests for reprints: Weibo Cai, PhD, Departments of Radiology and Medical Physics, University of Wisconsin - Madison, Room 7137, 1111 Highland Ave, Madison, WI 53705-2275, USA, wcai@uwhealth.org; Phone: 608-262-1749; Fax: 608- 265-0614.
[5]These authors contributed equally to this work

The authors declare no competing financial interest.

INTRODUCTION

Vascular endothelial growth factor (VEGF) is a potent mitogen in embryonic and somatic angiogenesis, the formation of new blood vessels.[1, 2] The VEGF/VEGF receptor (VEGFR) signaling pathway plays a crucial role in both normal vasculature development and disease processes such as tumor development and metastasis.[3, 4] VEGF-A is a homodimeric, disulfide-bound glycoprotein which exists in several isoforms with different numbers of amino acid residues, such as $VEGF_{121}$ and $VEGF_{165}$. Different VEGF-A isoforms exhibit varying biological properties such as the ability to bind to cell surface heparin sulfate proteoglycans. $VEGF_{121}$, commonly existing as a homodimer, is freely diffusible without heparin binding. The two VEGFRs, namely Flt-1 (VEGFR-1) and Flk-1/KDR (VEGFR-2), are endothelium-specific tyrosine kinase receptors that mediate most of the angiogenic actions of the VEGF family.[5] It has been reported that VEGFs and/or VEGFRs are overexpressed in various tumor biopsy specimens, which is indicative of poor prognosis for cancer patients.[2, 6, 7] Therefore, non-invasive imaging and quantification of VEGFR expression is of paramount importance in cancer patient management.

Many strategies have been adopted to block the VEGF/VEGFR signaling pathway for cancer treatment, such as agents that can bind to VEGF-A to prevent its interaction with VEGFRs (bevacizumab, VEGF-trap, etc.),[8, 9] antibodies/antibody fragments that target VEGFR-2 (ramucirumab, CDP791, etc.),[10, 11] and small molecule inhibitors that interrupt the downstream signaling of VEGFR-2 (axitinib, sunitinib, sorafenib, etc.).[12–14] Many of these agents have been approved by the Food and Drug Administration (FDA) for various medical indications in cancer therapy.[2, 15] Non-invasive imaging and measurement of VEGFR expression can provide important information in future anti-angiogenic drug development and clinical trials, such as patient stratification and evaluating the therapeutic response/efficacy. Due to the soluble and dynamic nature of VEGF proteins, imaging of VEGF expression was not studied as extensively as imaging of VEGFR expression.[3, 16] To date, the strategies used for VEGF imaging are almost exclusively based on anti-VEGF antibodies or reporter gene approaches.

Tremendous effort has been devoted to non-invasive imaging of VEGFR expression in cancer over the last two decades and various agents have been developed for different imaging modalities, such as single photon emission computed tomography (SPECT),[17–20] positron emission tomography (PET),[18, 21–25] optical imaging,[18, 26] magnetic resonance imaging (MRI),[27] and ultrasound.[28, 29] Because of the high affinity to VEGFRs, $VEGF_{121}$ has emerged as a particularly desirable candidate for tracer development in the literature.[3, 30] To avoid significant interference with VEGFR binding, site-specific labeling of VEGF-based proteins has been adopted in many literature reports which typically utilizes a cysteine residue for radiolabeling.[4,18] However, in many of the reported studies, kidney uptake of the tracer was very high (in some cases > 100 percentage of injected dose per gram of tissue [%ID/g]) which significantly hampered the clinical translation/applications of these tracers.

The goal of this study is to develop a PET tracer for the imaging of VEGFR expression using lysine-tagged recombinant human $VEGF_{121}$ (denoted as K_3-$VEGF_{121}$). The three lysine residues at the N-terminus, far from the VEGFR binding sites, can facilitate radiolabeling without affecting the biological activity and receptor binding. Since the commonly used PET isotope for protein labeling, ^{64}Cu, has low β^+ branching ratio (17%), in this study we used ^{61}Cu as a PET label which is ideal for small proteins like $VEGF_{121}$. The significantly shorter half-life than that of ^{64}Cu (3.3 h vs. 12.7 h) is more suitable for the pharmacokinetics of VEGF-based tracers and can give lower radiation dosimetry to normal organs. In addition, the much higher β^+ branching ratio of ^{61}Cu (62% vs. 17% for ^{64}Cu) leads to stronger signal intensity and requires lower injection dose of the PET tracer. These

features (shorter decay half-life, stronger signal, lower dose needed for PET imaging, etc.) are desirable for future clinical translation. In this work, K_3-$VEGF_{121}$ was conjugated to 2-S-(4-isothiocyanatobenzyl)-1,4,7-triazacyclononane-1,4,7-triacetic acid (p-SCN-Bn-NOTA) for ^{61}Cu labeling and in vivo investigation in a 4T1 murine breast cancer model.

EXPERIMENTAL SECTION

Reagents

K_3-$VEGF_{121}$ was synthesized through recombinant DNA technology and purified by GenScript Corp. (Piscataway, NJ). p-SCN-Bn-NOTA (Macrocyclics, Inc., Dallas, TX), PD-10 desalting columns (GE Healthcare, Piscataway, NJ), Chelex 100 resin (50–100 mesh; Sigma-Aldrich, St. Louis, MO), and FITC/Cy3-labeled secondary antibodies (Jackson Immunoresearch Laboratories, Inc., West Grove, CA) were all purchased from commercial sources. Water and all buffers were of Millipore grade and pre-treated with Chelex 100 resin to ensure that the aqueous solution was heavy metal-free. All other reaction buffers and chemicals were acquired from Thermo Fisher Scientific (Fair Lawn, NJ).

Cell Lines and Animal Model

4T1 murine breast cancer cells were purchased from the American Type Culture Collection (ATCC, Manassas, VA) and cultured in RPMI 1640 medium (Invitrogen, Carlsbad, CA) with 10% fetal bovine serum at 37 °C with 5% CO_2. Porcine aortic endothelial cells expressing human KDR (PAE/KDR) were cultured in Ham's F-12 medium containing 10% fetal calf serum. Cells were used for in vitro and in vivo experiments when they reached ~75% confluence. All animal studies were conducted under a protocol approved by the University of Wisconsin Institutional Animal Care and Use Committee. The 4T1 tumor model was generated by subcutaneous injection of 2×10^6 cells in 100 μl of phosphate-buffered saline (PBS) into the front flank of twelve-week-old female BALB/c mice (Harlan, Indianapolis, IN).[31] Tumor sizes were monitored every other day and mice were used for in vivo experiments when the diameter of tumors reached 5–8 mm (typically 1–2 weeks after inoculation).

NOTA-Conjugation, Cell Binding Assay, and ^{61}Cu-Labeling

NOTA-conjugation was carried out at pH 9.0 (in PBS adjusted with 0.1 N sodium carbonate), with the reaction ratio of p-SCN-Bn-NOTA:K_3-$VEGF_{121}$ being 10:1. NOTA-K_3-$VEGF_{121}$ was purified using PD-10 columns with PBS as the mobile phase. Detailed procedure for the cell-binding assay has been reported previously.[21, 22] VEGFR-2 binding affinity of K_3-$VEGF_{121}$ and NOTA-K_3-$VEGF_{121}$ was analyzed in PAE/KDR cells using ^{125}I-$VEGF_{165}$ as the radioligand.

^{61}Cu was produced in a GE PETtrace cyclotron using the ^{60}Ni(d,n)^{61}Cu reaction, with specific activity of ~2 Ci/μmol at the end of bombardment. $^{61}CuCl_2$ (74 MBq) was diluted in 300 μL of 0.1 M sodium acetate buffer (pH 5.5) and added to 10 μg of NOTA-K_3-$VEGF_{121}$ for radiolabeling. The reaction mixture was incubated for 30 min at 37 °C with constant shaking. ^{61}Cu-NOTA-K_3-$VEGF_{121}$ was purified using PD-10 columns with PBS as the mobile phase. The radioactive fractions containing ^{61}Cu-NOTA-K_3-$VEGF_{121}$ was collected and passed through a 0.2 μm syringe filter before in vivo experiments.

Imaging and Biodistribution Studies

PET/CT scans were performed using an Inveon microPET/microCT rodent model scanner (Siemens Medical Solutions USA, Inc.). Each 4T1 tumor-bearing mouse was intravenously injected with 3–5 MBq of ^{61}Cu-NOTA-K_3-$VEGF_{121}$ and five-minute static PET scans were performed at various time points post-injection (p.i.). Details for data acquisition, image

reconstruction, and region-of-interest (ROI) analysis have been reported previously.[32–34] Quantitative data were presented as %ID/g. Blocking studies were carried out to evaluate VEGFR specificity of ^{61}Cu-NOTA-K_3-$VEGF_{121}$ in vivo, where a group of four mice was each injected with ^{61}Cu-NOTA-K_3-$VEGF_{121}$ after intravenous injection of 100 μg of K_3-$VEGF_{121}$.

After the last PET scans at 8 h p.i., biodistribution studies were carried out to confirm that the quantitative tracer uptake values derived from PET imaging truly represented radioactivity distribution in tumor-bearing mice. Blood, 4T1 tumor, and major organs/tissues were collected and weighed. The radioactivity in each tissue was measured using a gamma-counter (Perkin Elmer) and presented as %ID/g. The 4T1 tumor, liver, and kidneys (i.e. tissues with significant uptake of ^{61}Cu-NOTA-K_3-$VEGF_{121}$) were also frozen for histological analysis.

Radiation Dosimetry Extrapolation to Humans

Estimated human dosimetry was calculated from serial PET imaging results on BALB/c female mice injected with ^{61}Cu-NOTA-K_3-$VEGF_{121}$. It was assumed that the biodistribution of the tracer in BALB/c mice was the same as in adult humans. ROI analysis was performed on major organs and time-activity curves were generated from the mean values obtained for each organ of interest. The source organ residence times were then calculated for the human model by integrating a mono-exponential fit to the experimental distribution data for major organs. Organ Level Internal Dose Assessment (OLINDA; Vanderbilt University) was used for estimating the radiation dosimetry.[35]

Histology

Frozen tissue slices of 5 μm thickness were fixed with cold acetone for 10 min and dried in the air for 30 min. After rinsing with PBS for 2 min and blocking with 10% donkey serum for 30 min at room temperature, the tissue slices were incubated with rabbit anti-mouse VEGFR-1 antibody (2 μg/mL, Thermo Fisher Lab Vision, Kalamazoo, MI) for 1 h at 4 °C and visualized using FITC-labeled donkey anti-rabbit secondary antibody. After washing with PBS, the slices were incubated with rat anti-mouse VEGFR-2 antibody (2 μg/mL) for 1 h at 4 °C and visualized with Cy3-conjugated donkey anti-rat secondary antibody. All images were acquired with a Nikon Eclipse Ti microscope.

Statistical Analysis

Quantitative data were expressed as mean ± SD. Means were compared using Student's t-test. P values < 0.05 were considered statistically significant.

RESULTS

In Vitro Studies

The amino acid sequence of K_3-$VEGF_{121}$ is shown in Figure 1A. Mass spectrometry indicated the expected molecular weight of ~14.6 kDa for K_3-$VEGF_{121}$ and another peak at ~29.3 kDa for the homodimer (Figure 1B). K_3-$VEGF_{121}$ exhibited > 95% purity as indicated by a Coomassie Blue-stained SDS-PAGE gel (Figure 1C), with a very light band of K_3-$VEGF_{121}$ homodimer above the 26 kDa marker band. The binding of K_3-$VEGF_{121}$ and NOTA-K_3-$VEGF_{121}$ to cells expressing VEGFR-2 was evaluated using ^{125}I-$VEGF_{165}$ as the competitive radioligand (Figure 1D). The measured 50% inhibitory concentration (IC_{50}) values of K_3-$VEGF_{121}$ and NOTA-K_3-$VEGF_{121}$ were 0.65 and 1.50 nM, respectively, indicating minimal interference with VEGFR-2 binding after NOTA conjugation. As a reference, the IC_{50} values of $VEGF_{121}$ were measured to be 1–3 nM in our previous studies using the same cell binding assay.[21, 22] This observation indicated that the lysine residues

used for NOTA conjugation were not within the VEGFR-2 binding domain (shown in blue in Figure 1A).[36] Through the addition of three lysine residues at the N-terminus of $VEGF_{121}$, which did not interfere with VEGFR-2 binding as indicated by the IC_{50} values, the possibility of modifying the lysine residue in the VEGFR-2 binding domain is significantly reduced.

^{61}Cu-Labeling

^{61}Cu-labeling including final purification using PD-10 columns took 60 ± 10 min (n = 8). The decay-corrected radiochemical yield was 55 ± 10 %, based on 5 μg of NOTA-K_3-$VEGF_{121}$ per 37 MBq of ^{61}Cu, with radiochemical purity of > 95%. The specific activity of ^{61}Cu-NOTA-K_3-$VEGF_{121}$ was 4.2 GBq/mg protein, assuming complete recovery of the NOTA-K_3-$VEGF_{121}$ conjugate after size exclusion chromatography.

Small Animal PET Imaging

Based on our previous studies on PET imaging of VEGFR expression with radiolabeled $VEGF_{121}$[21, 22] and the 3.3 h decay half-life of ^{61}Cu, the time points of 0.5, 2, 4, and 8 h p.i. were chosen for serial PET scans of 4T1 tumor-bearing mice after intravenous injection of ^{61}Cu-NOTA-K_3-$VEGF_{121}$. Coronal PET images that contain the 4T1 tumor are shown in Figure 2, with the quantitative data obtained from ROI analysis and representative PET/CT fused image of a mouse at 4 h p.i. of ^{61}Cu-NOTA-K_3-$VEGF_{121}$ shown in Figure 3.

^{61}Cu-NOTA-K_3-$VEGF_{121}$ cleared from the mouse body through both the hepatobiliary and renal pathways (with the former being more dominant). The uptake of ^{61}Cu-NOTA-K_3-$VEGF_{121}$ in the liver was prominent at early time points and decreased gradually over time. The %ID/g values of the liver was 35.2 ± 5.6, 27.4 ± 1.0, 27.4 ± 2.2, and 24.2 ±2.7 %ID/g at 0.5, 2, 4, and 8 h p.i. respectively (n = 4; Figure 3A). Importantly, the 4T1 tumor uptake of ^{61}Cu-NOTA-K_3-$VEGF_{121}$ was clearly visible starting from 2 h p.i. and remained stable over time (3.4 ± 0.5, 4.9 ± 1.0, 5.2 ± 1.0 and 4.8 ± 0.8 %ID/g at 0.5, 2, 4, and 8 h p.i. respectively; n = 4; Figure 2, 3A&C). Although the tumor uptake remained stable after 2 h p.i., the tumor-to-muscle ratio increased significantly from 2.6 ± 0.5 at 0.5 h p.i. to 4.9 ± 1.0 at 8 h p.i. (n = 4) due to tracer clearance from normal tissues.

Administering 100 μg of K_3-$VEGF_{121}$ at 30 min before ^{61}Cu-NOTA-K_3-$VEGF_{121}$ injection significantly reduced the tumor uptake ($P < 0.01$ at 2 and 4 h p.i. when compared with mice injected with ^{61}Cu-NOTA-K_3-$VEGF_{121}$ alone; Figure 2, 3B&C), indicating VEGFR specificity of the tracer in vivo. Radioactivity in the blood pool was comparably low for both groups. However, liver uptake of ^{61}Cu-NOTA-K_3-$VEGF_{121}$ in the “blocking” group (21.0 ± 0.4, 17.2 ± 0.8, 16.3 ± 2.3, and 14.8 ± 0.6 %ID/g at 0.5, 2, 4, and 8 h p.i. respectively; n = 4) was significantly lower at all time points examined ($P < 0.01$) than that of mice injected with ^{61}Cu-NOTA-K_3-$VEGF_{121}$ alone. Taken together, these data suggested faster renal/hepatic clearance of ^{61}Cu-NOTA-K_3-$VEGF_{121}$ when most VEGFR in the mice was already bound by pre-injected K_3-$VEGF_{121}$, thereby leaving fewer receptors available for the tracer to interact with. Successful blocking of the 4T1 tumor uptake with 100 μg/mouse of K_3-$VEGF_{121}$ confirmed the VEGFR specificity of ^{61}Cu-NOTA-K_3-$VEGF_{121}$ in vivo.

Biodistribution Studies and Radiation Dosimetry

All mice were euthanized after the last PET scans at 8 h p.i. The tissues were collected for biodistribution and immunofluorescence staining studies to validate the in vivo PET data. Figure 4 shows the biodistribution data of ^{61}Cu-NOTA-K_3-$VEGF_{121}$ at 8 h p.i. Besides the liver, the kidneys and intestine also had significant uptake of ^{61}Cu-NOTA-K_3-$VEGF_{121}$. Based on the biodistribution studies, the tumor-to-muscle ratio at 8 h p.i. was 5.9 ± 1.8 (n =

4) which is similar to that obtained from PET imaging (4.9 ± 1.0; n = 4). Pre-injection of a blocking dose of K_3-$VEGF_{121}$ led to a tumor-to-muscle ratio of 2.5 ± 0.4 (n = 4) at 8 h p.i., which was significantly lower than mice injected with ^{61}Cu-NOTA-K_3-$VEGF_{121}$ alone ($P < 0.05$) and corroborated the in vivo PET findings. Overall, the quantitative results obtained from biodistribution studies and PET scans matched very well, confirming that quantitative ROI analysis of non-invasive PET scans truly reflected tracer distribution in vivo.

Estimated human absorbed doses to normal organs from ^{61}Cu-NOTA-K_3-$VEGF_{121}$ are presented in Table 1. The highest radiation-absorbed dose is to the liver (0.23 ± 0.022 mGy/MBq; n = 4) and most other organs have very low level of radiation-absorbed doses. When compared to our previous studies on ^{64}Cu-DOTA-$VEGF_{121}$,[21] the radiation doses to most normal organs (e.g. brain, stomach, lungs, ovaries, spleen, uterus, etc.) were much lower. For the kidney which were the dose-limiting organ for ^{64}Cu-DOTA-$VEGF_{121}$ (1.05 ± 0.27 mGy/MBq, n = 3), this is not the case for ^{61}Cu-NOTA-K_3-$VEGF_{121}$ due to much lower kidney uptake of the tracer. The whole-body absorbed dose was found to be 0.024 ± 0.001 mGy/MBq administered ^{61}Cu-NOTA-K_3-$VEGF_{121}$, which is less than half of that for ^{64}Cu-DOTA-$VEGF_{121}$ (0.05 ± 0.006 mGy/MBq; n = 3). Together, the much improved estimated human dosimetry of ^{61}Cu-NOTA-K_3-$VEGF_{121}$ over ^{64}Cu-DOTA-$VEGF_{121}$ suggested that the use of ^{61}Cu as the PET isotope was more advantageous than ^{64}Cu for labeling small proteins such as $VEGF_{121}$ derivatives. The three additional lysine residues at the N-terminus may also have contributed to the more desirable biodistribution of the tracer, in addition to facilitating the radiolabeling procedure.

Histology

The frozen tissue slices of 4T1 tumor, liver, and kidneys were stained for VEGFR-1 and VEGFR-2 after decay of the radioactivity. High VEGFR-2 expression and detectable VEGFR-1 expression was observed in the 4T1 tumor (Figure 5), which corresponded to prominent tracer uptake within the tumor. The observable level of VEGFR-2, but not VEGFR-1, expression in the liver and kidneys may also have contributed partly to tracer accumulation in these two organs. However, the majority of ^{61}Cu-NOTA-K_3-$VEGF_{121}$ uptake in the liver and kidneys is likely related to hepatic/renal clearance, nonspecific capture, and possibly metabolites of the tracer after VEGFR-mediated internalization into cells.

DISCUSSION

PET imaging has been widely for patient management in clinical oncology.[37–39] Non-invasive imaging of VEGFR expression holds enormous potential to accelerate anti-angiogenic drug development and improve the management of cancer patients.[3, 4, 30] In this study, we developed a PET tracer by labeling lysine-tagged $VEGF_{121}$ with ^{61}Cu for imaging of VEGFR expression in a murine breast cancer model and demonstrated the specificity of ^{61}Cu-NOTA-K_3-$VEGF_{121}$ in vitro, in vivo and ex vivo. Many radiotracers have been reported for in vivo imaging of VEGFR expression previously,[3, 4, 30] among which $VEGF_{121}$ was one of the most popular ligands used for tracer development. However, direct labeling of $VEGF_{121}$ for VEGFR imaging faces several challenges such as potential interference with the VEGFR-2 binding affinity (VEGFR-1 binding is of less concern for cancer imaging since VEGFR-2 has been shown to be more important than VEGFR-1 for tumor angiogenesis[2, 22]), very high renal uptake in mouse models which hampers clinical translation,[3] the choice of the optimal PET isotope, in vivo stability of the PET label, among others. Our study addresses several of these issues and ^{61}Cu-NOTA-K_3-$VEGF_{121}$ exhibits many desirable characteristics for future clinical translation.

There are 10 lysine residues in K_3-$VEGF_{121}$, with 3 at the N-terminus and 7 in the naturally occurring $VEGF_{121}$. Among these lysine residues that are amenable for radiolabeling, Lys^{84} is critical for VEGFR-2 binding and should not be modified in order to preserve VEGFR-2 binding affinity.[36] By adding 3 lysine residues at the N-terminus, the possibility of compromising the biological activity of $VEGF_{121}$ after NOTA conjugation is significantly reduced. With the reaction ratio of p-SCN-Bn-NOTA:K_3-$VEGF_{121}$ being 10:1, it was estimated that there are 1~2 NOTA residues in each NOTA-K_3-$VEGF_{121}$. Such minimum modification of the protein did not alter the binding affinity of $VEGF_{121}$ to VEGFR-2, as cell binding assay confirmed that the IC_{50} values of both K_3-$VEGF_{121}$ and NOTA-K_3-$VEGF_{121}$ were comparable to the naturally occurring $VEGF_{121}$ at the nM range. The in vivo and ex vivo experiments further confirmed the binding affinity and target specificity of the tracer.

Radiation dose to both patients and healthcare personnel is a major concern for radiopharmaceuticals.[40–42] In the design of novel radiotracers, it is important to minimize the radiation dose to normal organs without compromising the imaging characteristics. $VEGF_{121}$ and its derivatives have been labeled with many PET/SPECT isotopes.[3, 4, 30] However, some tracers resulted in relatively low tumor uptake, while several others showed high radiation dose to normal organs such as kidneys and the liver. ^{61}Cu, with a 3.3 h decay half-life, 62% β^+ branch ratio, and 1.22 MeV maximum β^+ energy, is an excellent PET isotope for labeling of small molecules or proteins. However, development of ^{61}Cu-based PET tracers has been severely understudied due to limited commercial availability of the isotope, despite the fact that tumor images obtained using ^{61}Cu were found to be superior to those using ^{64}Cu.[43] The relatively short half-life and high β^+ branch ratio requires lower radiotracer dose for imaging applications and can lead to shorter organ residence time than other PET isotopes such as ^{64}Cu. In our study, the liver was the organ with the highest radiation dose (which is still at a relatively low level) because ^{61}Cu-NOTA-K_3-$VEGF_{121}$ was cleared from mice primarily through the hepatic route. The estimated radiation doses to the other normal organs were even lower, which makes this tracer suitable for future clinical translation.

In comparison with the clinical “gold standard” PET isotope ^{18}F, which is typically time consuming for protein labeling and often gives low radiochemical yield,[40, 44] labeling K_3-$VEGF_{121}$ with ^{61}Cu was achieved rapidly (~ 30 minutes) with good yield (> 50%). In addition, radiometal can often give higher tumor uptake than similar ^{18}F-labeled tracers, due to much higher intracellular trapping efficiency of the radiometal than ^{18}F after receptor-mediated internalization of the tracer into tumor (vascular endothelial) cells and subsequent metabolism.[45] The 4T1 tumor uptake of ^{61}Cu-NOTA-K_3-$VEGF_{121}$ reached > 5 %ID/g at 4 h p.i. in our study, which gave good tumor contrast. Even though ^{61}Cu is not commercially available yet, it is feasible to distribute it to sites without a cyclotron similar as how ^{18}F and ^{18}F-FDG are currently supplied through commercial carriers, once the broad clinical potential of ^{61}Cu is demonstrated. Of note, cyclotron production of ^{61}Cu has a relatively low cost with the use of a deuteron beam for ^{61}Cu production (^{60}Ni is significantly less expensive than ^{64}Ni, which are commonly used for ^{64}Cu production with a proton beam). For imaging/diagnostic purposes using radiolabeled small proteins, ^{61}Cu is a preferred choice over the more widely available ^{64}Cu. Several other PET isotopes also have desirable characteristics for protein-based imaging (e.g. ^{45}Ti and ^{44}Sc, both with similar half-lives as ^{61}Cu and higher β^+ branching ratio), which deserve more research effort in the near future. Since the tumor uptake of ^{61}Cu-NOTA-K_3-$VEGF_{121}$ peaks at around 4 h p.i., ^{68}Ga is not suitable for labeling of K_3-$VEGF_{121}$ because of its short decay half-life (68.3 minutes). Furthermore, the much higher energy of β^+ emitted by ^{68}Ga will also lead to lower quality PET images than ^{61}Cu-based tracers.

The in vivo stability of radiometal-based tracers is always a concern, such as those based on copper radioisotopes. An elegant study compared the effect of several bifunctional chelators on the biodistribution of a ^{64}Cu-labeled antibody,[46] which concluded that thermodynamic stability of ^{64}Cu-chelator complexes did not significantly influence tumor uptake of the tracer. However, there were significant differences in tracer concentration in other tissues, including those involved in tracer clearance (e.g. liver and spleen). Similar findings were also observed in our previous studies of ^{64}Cu-based tracers[34, 47] and it is now generally agreed that NOTA is one of the best chelators for $^{61/64}$Cu-labeling of proteins,[46, 48] which was used in this work.

The endogenous isoforms of VEGF may compete with ^{61}Cu-NOTA-K_3-$VEGF_{121}$, which can potentially influence tracer uptake in the tumor and makes quantitative correlation of VEGFR expression with tracer uptake more difficult. Nonetheless, the intact VEGFR binding affinity of NOTA-K_3-$VEGF_{121}$ and the fact that the endogenous VEGF concentration is far from saturating the VEGFR resulted in prominent ^{61}Cu-NOTA-K_3-$VEGF_{121}$ uptake in the 4T1 tumors. Lastly, rodent kidneys typically express significant level of VEGFR-1 during development which can cause very high renal uptake of VEGF-based tracers in mouse models,[21, 22] since $VEGF_{121}$ binds to VEGFR-1 with higher affinity than VEGFR-2. Such VEGFR-1 expression in rodent kidneys is age dependent. With the use of adult mice (12–14 weeks) in this study, the kidney uptake is acceptable (~10 %ID/g) and much lower than previous studies of VEGF-based tracers (usually > 30%ID/g).[3, 21] It is likely that the use of these mice is more clinically relevant since most cancer patients are adults. Furthermore, VEGFR-1 expression in human kidneys is not as prominent as that in rodents.

CONCLUSION

We have successfully synthesized ^{61}Cu-labeled K_3-$VEGF_{121}$, a recombinant $VEGF_{121}$ with three lysine residues fused to the N-terminus to facilitate radiolabeling without compromising its biological activity. The binding affinity, tumor targeting efficiency, and VEGFR specificity of the tracer was investigated both in vitro and in vivo. Small animal PET imaging revealed fast, prominent, and VEGFR-specific uptake of ^{61}Cu-NOTA-K_3-$VEGF_{121}$ in the 4T1 tumor model, which were validated by biodistribution, blocking, and histology studies. By using ^{61}Cu as the PET isotope, the estimated radiation dose to humans could be significantly reduced when compared with similar ^{64}Cu-labeled tracers. In addition, high β^+ branching ratio and desirable half-life of ^{61}Cu also makes the tracer suitable for future investigations in multiple scenarios such as clinical translation and evaluating the biological responses to various anti-cancer drugs.

Acknowledgments

The authors acknowledge financial support from the University of Wisconsin Carbone Cancer Center, the Department of Defense (W81XWH-11-1-0644), and the Elsa U. Pardee Foundation.

References

1. Ferrara N. VEGF and the quest for tumour angiogenesis factors. Nat Rev Cancer. 2002; 2:795–803. [PubMed: 12360282]
2. Ferrara N. Vascular endothelial growth factor: basic science and clinical progress. Endocr Rev. 2004; 25:581–611. [PubMed: 15294883]
3. Cai W, Chen X. Multimodality imaging of vascular endothelial growth factor and vascular endothelial growth factor receptor expression. Front Biosci. 2007; 12:4267–79. [PubMed: 17485373]

4. Backer MV, Backer JM. Imaging key biomarkers of tumor angiogenesis. Theranostics. 2012; 2:502–15. [PubMed: 22737188]
5. Sato Y, Kanno S, Oda N, Abe M, Ito M, Shitara K, Shibuya M. Properties of two VEGF receptors, Flt-1 and KDR, in signal transduction. Ann N Y Acad Sci. 2000; 902:201–5. discussion 205–7. [PubMed: 10865839]
6. Underiner TL, Ruggeri B, Gingrich DE. Development of vascular endothelial growth factor receptor (VEGFR) kinase inhibitors as anti-angiogenic agents in cancer therapy. Curr Med Chem. 2004; 11:731–45. [PubMed: 15032727]
7. Decaussin M, Sartelet H, Robert C, Moro D, Claraz C, Brambilla C, Brambilla E. Expression of vascular endothelial growth factor (VEGF) and its two receptors (VEGF-R1-Flt1 and VEGF-R2-Flk1/KDR) in non-small cell lung carcinomas (NSCLCs): correlation with angiogenesis and survival. J Pathol. 1999; 188:369–77. [PubMed: 10440746]
8. Ferrara N, Hillan KJ, Gerber HP, Novotny W. Discovery and development of bevacizumab, an anti-VEGF antibody for treating cancer. Nat Rev Drug Discov. 2004; 3:391–400. [PubMed: 15136787]
9. Moroney JW, Sood AK, Coleman RL. Aflibercept in epithelial ovarian carcinoma. Future Oncol. 2009; 5:591–600. [PubMed: 19519199]
10. Spratlin JL, Cohen RB, Eadens M, Gore L, Camidge DR, Diab S, Leong S, O'Bryant C, Chow LQ, Serkova NJ, Meropol NJ, Lewis NL, Chiorean EG, Fox F, Youssoufian H, Rowinsky EK, Eckhardt SG. Phase I pharmacologic and biologic study of ramucirumab (IMC-1121B), a fully human immunoglobulin G1 monoclonal antibody targeting the vascular endothelial growth factor receptor-2. J Clin Oncol. 2010; 28:780–7. [PubMed: 20048182]
11. Ton NC, Parker GJ, Jackson A, Mullamitha S, Buonaccorsi GA, Roberts C, Watson Y, Davies K, Cheung S, Hope L, Power F, Lawrance J, Valle J, Saunders M, Felix R, Soranson JA, Rolfe L, Zinkewich-Peotti K, Jayson GC. Phase I evaluation of CDP791, a PEGylated di-Fab' conjugate that binds vascular endothelial growth factor receptor 2. Clin Cancer Res. 2007; 13:7113–8. [PubMed: 18056191]
12. Fruehauf J, Lutzky J, McDermott D, Brown CK, Meric JB, Rosbrook B, Shalinsky DR, Liau KF, Niethammer AG, Kim S, Rixe O. Multicenter, phase II study of axitinib, a selective second-generation inhibitor of vascular endothelial growth factor receptors 1, 2, and 3, in patients with metastatic melanoma. Clin Cancer Res. 2011; 17:7462–9. [PubMed: 21976544]
13. Motzer RJ, Michaelson MD, Redman BG, Hudes GR, Wilding G, Figlin RA, Ginsberg MS, Kim ST, Baum CM, DePrimo SE, Li JZ, Bello CL, Theuer CP, George DJ, Rini BI. Activity of SU11248, a multitargeted inhibitor of vascular endothelial growth factor receptor and platelet-derived growth factor receptor, in patients with metastatic renal cell carcinoma. J Clin Oncol. 2006; 24:16–24. [PubMed: 16330672]
14. Strumberg D, Richly H, Hilger RA, Schleucher N, Korfee S, Tewes M, Faghih M, Brendel E, Voliotis D, Haase CG, Schwartz B, Awada A, Voigtmann R, Scheulen ME, Seeber S. Phase I clinical and pharmacokinetic study of the Novel Raf kinase and vascular endothelial growth factor receptor inhibitor BAY 43-9006 in patients with advanced refractory solid tumors. J Clin Oncol. 2005; 23:965–72. [PubMed: 15613696]
15. Folkman J. Angiogenesis: an organizing principle for drug discovery? Nat Rev Drug Discov. 2007; 6:273–86. [PubMed: 17396134]
16. Cai W, Hong H. Peptoid and positron emission tomography: an appealing combination. Am J Nucl Med Mol Imaging. 2011; 1:76–79. [PubMed: 22022661]
17. Chan C, Sandhu J, Guha A, Scollard DA, Wang J, Chen P, Bai K, Lee L, Reilly RM. A human transferrin-vascular endothelial growth factor (hnTf-VEGF) fusion protein containing an integrated binding site for ^{111}In for imaging tumor angiogenesis. J Nucl Med. 2005; 46:1745–52. [PubMed: 16204726]
18. Backer MV, Levashova Z, Patel V, Jehning BT, Claffey K, Blankenberg FG, Backer JM. Molecular imaging of VEGF receptors in angiogenic vasculature with single-chain VEGF-based probes. Nat Med. 2007; 13:504–9. [PubMed: 17351626]
19. Blankenberg FG, Backer MV, Levashova Z, Patel V, Backer JM. In vivo tumor angiogenesis imaging with site-specific labeled ^{99m}Tc-HYNIC-VEGF. Eur J Nucl Med Mol Imaging. 2006; 33:841–8. [PubMed: 16699765]

20. Li S, Peck-Radosavljevic M, Kienast O, Preitfellner J, Havlik E, Schima W, Traub-Weidinger T, Graf S, Beheshti M, Schmid M, Angelberger P, Dudczak R. Iodine-123-vascular endothelial growth factor-165 (^{123}I-VEGF$_{165}$). Biodistribution, safety and radiation dosimetry in patients with pancreatic carcinoma. Q J Nucl Med Mol Imaging. 2004; 48:198–206. [PubMed: 15499293]
21. Cai W, Chen K, Mohamedali KA, Cao Q, Gambhir SS, Rosenblum MG, Chen X. PET of vascular endothelial growth factor receptor expression. J Nucl Med. 2006; 47:2048–56. [PubMed: 17138749]
22. Wang H, Cai W, Chen K, Li ZB, Kashefi A, He L, Chen X. A new PET tracer specific for vascular endothelial growth factor receptor 2. Eur J Nucl Med Mol Imaging. 2007; 34:2001–10. [PubMed: 17694307]
23. Hsu AR, Cai W, Veeravagu A, Mohamedali KA, Chen K, Kim S, Vogel H, Hou LC, Tse V, Rosenblum MG, Chen X. Multimodality molecular imaging of glioblastoma growth inhibition with vasculature-targeting fusion toxin VEGF$_{121}$/rGel. J Nucl Med. 2007; 48:445–54. [PubMed: 17332623]
24. Eder M, Krivoshein AV, Backer M, Backer JM, Haberkorn U, Eisenhut M. ScVEGF-PEG-HBED-CC and scVEGF-PEG-NOTA conjugates: comparison of easy-to-label recombinant proteins for [^{68}Ga]PET imaging of VEGF receptors in angiogenic vasculature. Nucl Med Biol. 2010; 37:405–12. [PubMed: 20447550]
25. Wang H, Gao H, Guo N, Niu G, Ma Y, Kiesewetter DO, Chen X. Site-Specific Labeling of scVEGF with Fluorine-18 for Positron Emission Tomography Imaging. Theranostics. 2012; 2:607–617. [PubMed: 22768028]
26. Wang H, Chen K, Niu G, Chen X. Site-specifically biotinylated VEGF$_{121}$ for near-infrared fluorescence imaging of tumor angiogenesis. Mol Pharm. 2009; 6:285–94. [PubMed: 19099493]
27. De Leon-Rodriguez LM, Lubag A, Udugamasooriya DG, Proneth B, Brekken RA, Sun X, Kodadek T, Dean Sherry A. MRI detection of VEGFR2 in vivo using a low molecular weight peptoid-(Gd)8-dendron for targeting. J Am Chem Soc. 2010; 132:12829–31. [PubMed: 20795620]
28. Willmann JK, Paulmurugan R, Chen K, Gheysens O, Rodriguez-Porcel M, Lutz AM, Chen IY, Chen X, Gambhir SS. US imaging of tumor angiogenesis with microbubbles targeted to vascular endothelial growth factor receptor type 2 in mice. Radiology. 2008; 246:508–18. [PubMed: 18180339]
29. Korpanty G, Carbon JG, Grayburn PA, Fleming JB, Brekken RA. Monitoring response to anticancer therapy by targeting microbubbles to tumor vasculature. Clin Cancer Res. 2007; 13:323–30. [PubMed: 17200371]
30. Cai W, Chen X. Multimodality molecular imaging of tumor angiogenesis. J Nucl Med. 2008; 49(Suppl 2):113S–28S. [PubMed: 18523069]
31. Hong H, Yang Y, Zhang Y, Engle JW, Barnhart TE, Nickles RJ, Leigh BR, Cai W. Positron emission tomography imaging of CD105 expression during tumor angiogenesis. Eur J Nucl Med Mol Imaging. 2011; 38:1335–43. [PubMed: 21373764]
32. Zhang Y, Hong H, Engle JW, Yang Y, Barnhart TE, Cai W. Positron Emission Tomography and Near-Infrared Fluorescence Imaging of Vascular Endothelial Growth Factor with Dual-Labeled Bevacizumab. Am J Nucl Med Mol Imaging. 2012; 2:1–13. [PubMed: 22229128]
33. Zhang Y, Hong H, Engle JW, Yang Y, Theuer CP, Barnhart TE, Cai W. Positron Emission Tomography and Optical Imaging of Tumor CD105 Expression with a Dual-Labeled Monoclonal Antibody. Mol Pharm. 2012; 9:645–53. [PubMed: 22292418]
34. Hong H, Benink HA, Zhang Y, Yang Y, Uyeda HT, Engle JW, Severin GW, McDougall MG, Barnhart TE, Klaubert DH, Nickles RJ, Fan F, Cai W. HaloTag: a novel reporter gene for positron emission tomography. Am J Transl Res. 2011; 3:392–403. [PubMed: 21904659]
35. Sgouros G. Dosimetry of internal emitters. J Nucl Med. 2005; 46(Suppl 1):18S–27S. [PubMed: 15653648]
36. Keyt BA, Nguyen HV, Berleau LT, Duarte CM, Park J, Chen H, Ferrara N. Identification of vascular endothelial growth factor determinants for binding KDR and FLT-1 receptors. Generation of receptor-selective VEGF variants by site-directed mutagenesis. J Biol Chem. 1996; 271:5638–46. [PubMed: 8621427]

37. Eary JF, Hawkins DS, Rodler ET, Conrad EUI. ^{18}F-FDG PET in sarcoma treatment response imaging. Am J Nucl Med Mol Imaging. 2011; 1:47–53. [PubMed: 23133794]
38. Grassi I, Nanni C, Allegri V, Morigi JJ, Montini GC, Castellucci P, Fanti S. The clinical use of PET with ^{11}C-acetate. Am J Nucl Med Mol Imaging. 2012; 2:33–47. [PubMed: 23133801]
39. Iagaru A. ^{18}F-FDG PET/CT: timing for evaluation of response to therapy remains a clinical challenge. Am J Nucl Med Mol Imaging. 2011; 1:63–64. [PubMed: 23133796]
40. Nolting DD, Nickels ML, Guo N, Pham W. Molecular imaging probe development: a chemistry perspective. Am J Nucl Med Mol Imaging. 2012; 2:273–306. [PubMed: 22943038]
41. Thorek DLJ, Robertson R, Bacchus WA, Hahn J, Rothberg J, Beattie BJ, Grimm J. Cerenkov imaging - a new modality for molecular imaging. Am J Nucl Med Mol Imaging. 2012; 2:163–173. [PubMed: 23133811]
42. Zhang L, Chang RC, Chu L, Mak HK. Current neuroimaging techniques in Alzheimer's disease and applications in animal models. Am J Nucl Med Mol Imaging. 2012; 2:386–404. [PubMed: 23133824]
43. McCarthy DW, Bass LA, Cutler PD, Shefer RE, Klinkowstein RE, Herrero P, Lewis JS, Cutler CS, Anderson CJ, Welch MJ. High purity production and potential applications of copper-60 and copper-61. Nucl Med Biol. 1999; 26:351–8. [PubMed: 10382836]
44. Alauddin MM. Positron emission tomography (PET) imaging with ^{18}F-based radiotracers. Am J Nucl Med Mol Imaging. 2012; 2:55–76. [PubMed: 23133802]
45. Cai W, Niu G, Chen X. Imaging of integrins as biomarkers for tumor angiogenesis. Curr Pharm Des. 2008; 14:2943–73. [PubMed: 18991712]
46. Dearling JLJ, Voss SD, Dunning P, Snay E, Fahey F, Smith SV, Huston JS, Meares CF, Treves ST, Packard AB. Imaging cancer using PET -- the effect of the bifunctional chelator on the biodistribution of a ^{64}Cu-labeled antibody. Nucl Med Biol. 2011; 38:29–38. [PubMed: 21220127]
47. Zhang Y, Hong H, Engle JW, Bean J, Yang Y, Leigh BR, Barnhart TE, Cai W. Positron emission tomography imaging of CD105 expression with a ^{64}Cu-labeled monoclonal antibody: NOTA is superior to DOTA. PLoS One. 2011; 6:e28005. [PubMed: 22174762]
48. Cooper MS, Ma MT, Sunassee K, Shaw KP, Williams JD, Paul RL, Donnelly PS, Blower PJ. Comparison of ^{64}Cu-Complexing Bifunctional Chelators for Radioimmunoconjugation: Labeling Efficiency, Specific Activity, and in Vitro/in Vivo Stability. Bioconjug Chem. 2012; 23:1029–1039. [PubMed: 22471317]

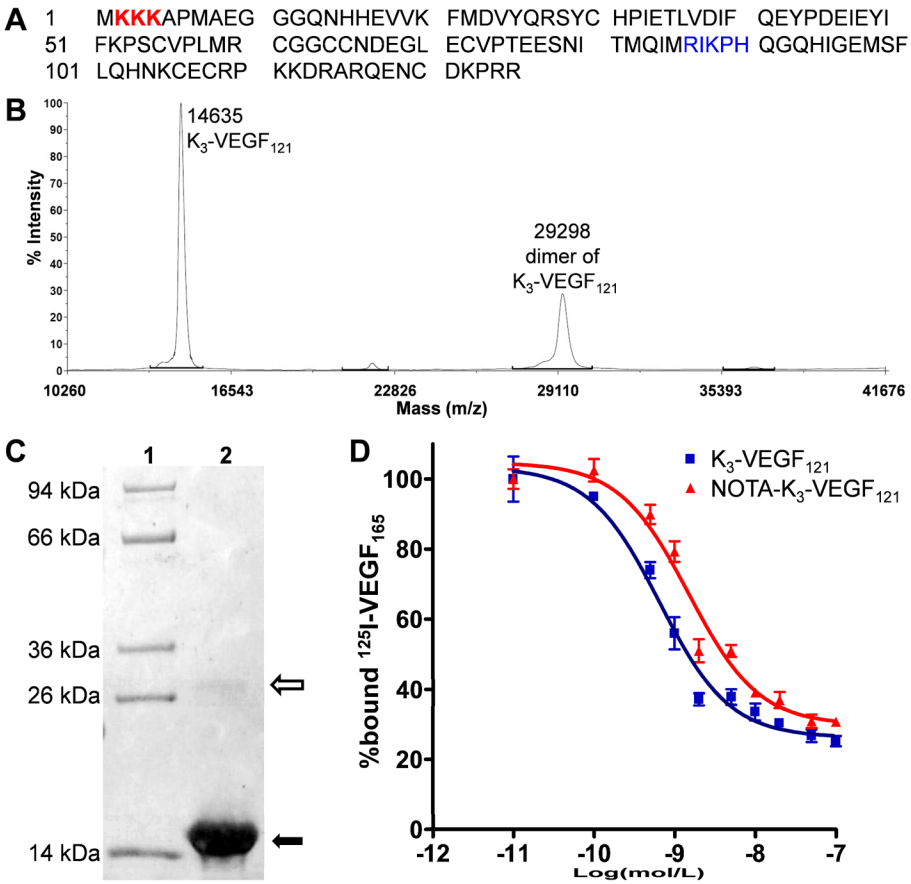

Figure 1.

Characterization of K_3-$VEGF_{121}$ and NOTA-K_3-$VEGF_{121}$. (A) The amino acid sequence of K_3-$VEGF_{121}$. The 3 added lysine residues are coded in red and the amino acid residues involved in VEGFR-2 binding are shown in blue, which contain a lysine residue. (B) Mass spectrometry of K_3-$VEGF_{121}$ which shows the expected peak (14635 Da) as well as the homodimer (29298 Da). (C) SDS-PAGE gel indicated > 95% purity of K_3-$VEGF_{121}$ (solid arrow) with a very light homodimer band (empty arrow). Lane 1: molecular weight marker; Lane 2: K_3-$VEGF_{121}$. (D) Cell binding assay in PAE/KDR cells with ^{125}I-$VEGF_{165}$ as the competitive ligand. Data represent triplicate samples. The IC_{50} values are 0.65 and 1.50 nM for K_3-$VEGF_{121}$ and NOTA-K_3-$VEGF_{121}$, respectively.

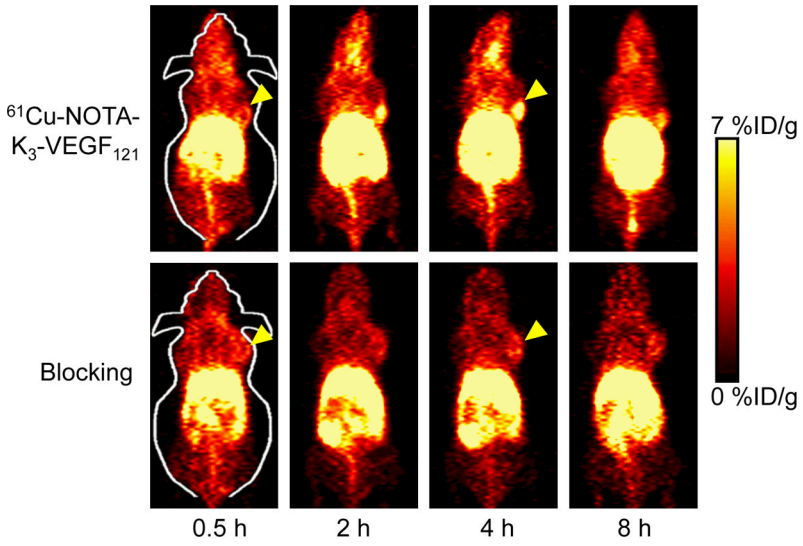

Figure 2.

Serial coronal PET images of 4T1 tumor-bearing mice at 0.5, 2, 4, and 8 h post-injection of ^{61}Cu-NOTA-K$_3$-VEGF$_{121}$, or a 100 μg dose of K$_3$-VEGF$_{121}$ before ^{61}Cu-NOTA-K$_3$-VEGF$_{121}$ administration (i.e. blocking). Images are representative of 4 mice per group and the 4T1 tumors are indicated by arrowheads.

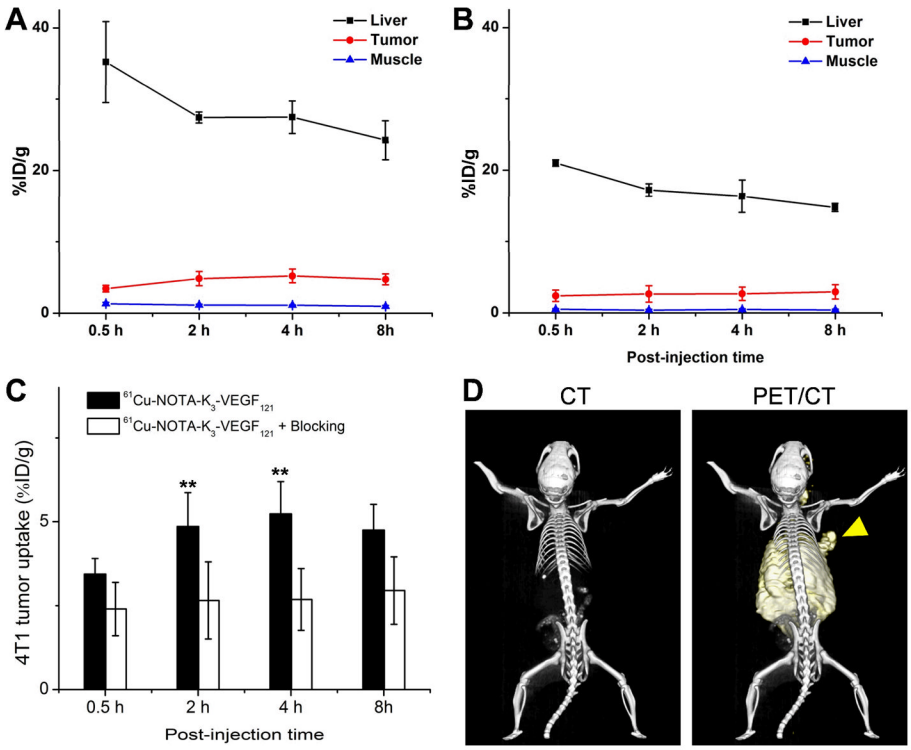

Figure 3.

Quantitative analysis of the PET data. (A) Time-activity curves of the liver, 4T1 tumor, and muscle upon intravenous injection of ^{61}Cu-NOTA-K$_3$-VEGF$_{121}$ into 4T1 tumor-bearing mice (n = 4). (B) Time-activity curves of the liver, 4T1 tumor, and muscle upon intravenous injection of ^{61}Cu-NOTA-K$_3$-VEGF$_{121}$, after a 100 μg dose of K$_3$-VEGF$_{121}$, into 4T1 tumor-bearing mice (n = 4). (C) Comparison of 4T1 tumor uptake between the two groups (n = 4). D. Representative PET/CT images of a 4T1 tumor-bearing mouse at 4 h post-injection of ^{61}Cu-NOTA-K$_3$-VEGF$_{121}$. Arrowhead indicates the tumor. **: $P < 0.01$.

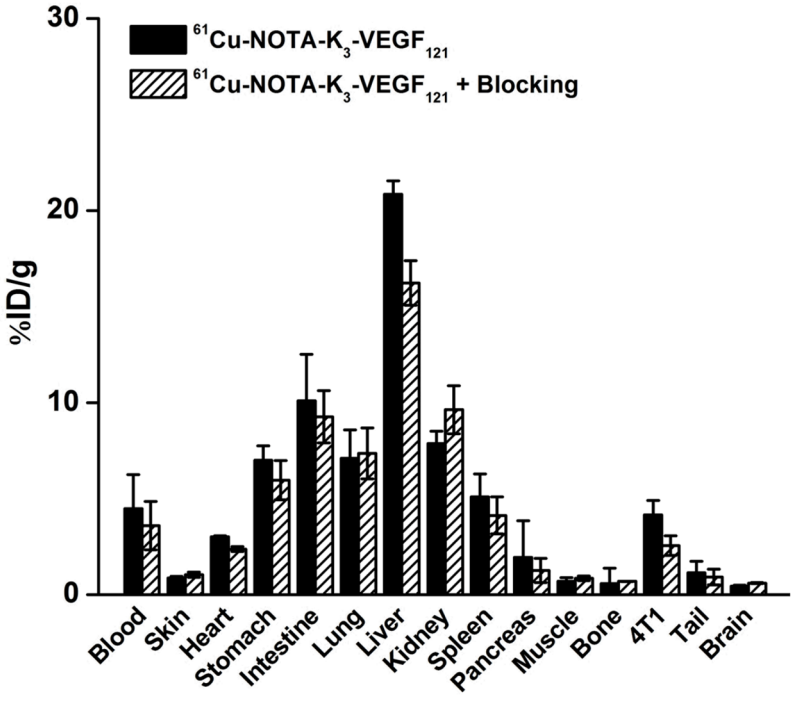

Figure 4.

Biodistribution data in 4T1 tumor-bearing mice at 8 h post-injection of ^{61}Cu-NOTA-K_3-$VEGF_{121}$, or ^{61}Cu-NOTA-K_3-$VEGF_{121}$ after a 100 μg pre-injected dose of K_3-$VEGF_{121}$. n = 4 per group.

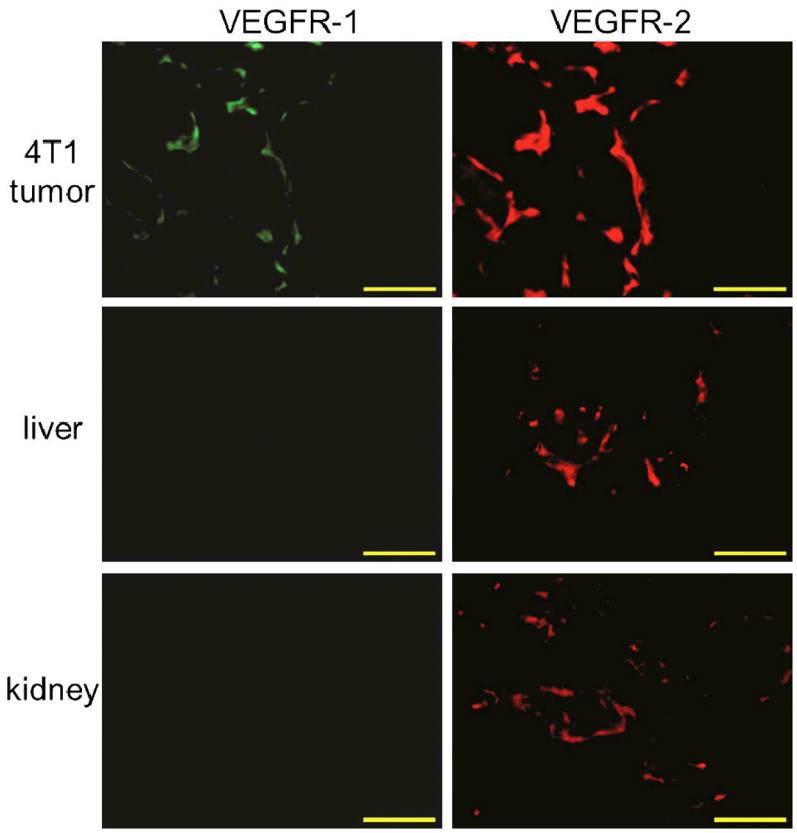

Figure 5.
Immunofluorescence VEGFR-1/VEGFR-2 staining of the 4T1 tumor, liver, and kidney tissue sections. All images were acquired under the same conditions and displayed at the same scale. Magnification: 200×. Scale bar: 50 μm.

TABLE 1

Estimated radiation absorbed doses to an adult human after intravenous injection of ^{61}Cu-NOTA-K_3-$VEGF_{121}$ based on PET imaging data obtained in female mice (n = 4).

Organ	mGy/MBq (SO)	rad/mCi (SO)
Adrenals	2.25E-02 (1.15E-03)	8.33E-02 (4.24E-03)
Brain	1.54E-04 (1.51E-05)	5.71E-04 (5.53E-05)
Breasts	4.49E-03 (7.14E-04)	1.66E-02 (2.63E-03)
Gallbladder	3.28E-02 (1.68E-03)	1.22E-01 (6.35E-03)
LLI Wall	5.08E-03 (2.34E-03)	1.88E-02 (8.64E-03)
Small Intestine	6.93E-02 (4.28E-02)	2.57E-01 (1.59E-01)
Stomach	9.88E-03 (2.60E-04)	3.66E-02 (9.95E-04)
ULI Wall	1.62E-02 (4.96E-03)	5.98E-02 (1.83E-02)
Heart	6.33E-02 (2.52E-02)	2.34E-01 (9.33E-02)
Kidneys	2.04E-01 (8.68E-03)	7.54E-01 (3.29E-02)
Liver	2.29E-01 (2.17E-02)	8.47E-01 (8.07E-02)
Lungs	1.03E-02 (1.41E-03)	3.82E-02 (5.21E-03)
Muscle	5.43E-03 (1.55E-04)	2.01E-02 (5.89E-04)
Ovaries	7.67E-03 (3.42E-03)	2.84E-02 (1.27E-02)
Pancreas	1.85E-02 (9.11E-04)	6.83E-02 (3.44E-03)
Skin	6.11E-03 (3.72E-04)	2.26E-02 (1.37E-03)
Spleen	4.30E-03 (1.03E-04)	1.59E-02 (3.74E-04)
Thymus	2.46E-03 (7.75E-05)	9.10E-03 (2.74E-04)
Thyroid	1.02E-02 (1.70E-04)	3.77E-02 (6.50E-04)
Urinary	6.27E-03 (1.72E-03)	2.32E-02 (6.35E-03)
Uterus	1.01E-03 (1.45E-04)	3.72E-03 (5.35E-04)
Effective dose	2.42E-02 (1.04E-03)	8.96E-02 (3.14E-03)

LLI = lower large intestine; ULI = upper large intestine.